2021-07

Using time series of MODIS land surface phenology to model temperature and photoper...

This work was made openly accessible by BU Faculty. Please share how this access benefits you. Your story matters.

1 **Using Time Series of MODIS Land Surface Phenology to Model Temperature and**

2 **Photoperiod Controls on Spring Greenup in North American Deciduous Forests**

3

4

5 Minkyu Moon[1*], Bijan Seyednasrollah[2,3], Andrew D. Richardson[2,3], Mark A. Friedl[1]

6

7 [1]Department of Earth and Environment, Boston University

8 [2]School of Informatics, Computing, and Cyber Systems, Northern Arizona University

9 [3]Center for Ecosystem Science and Society, Northern Arizona University

10 *Corresponding author: 685 Commonwealth Avenue, Boston, MA 02215, USA

11 E-mail address: moon.minkyu@gmail.com (Minkyu Moon)

12

13   **Abstract**

14   The timing of leaf emergence in temperate and boreal forests is changing, which has

15   profound implications for a wide array of ecosystem processes and services. Spring phenology

16   models, which have been widely used to predict the timing of leaf emergence, generally assume

17   that a combination of photoperiod and thermal forcing control when leaves emerge. However,

18   the exact nature and magnitude of how photoperiod and temperature individually and jointly

19   control leaf emergence is the subject of ongoing debate. Here we use a continuous development

20   model in combination with time series of land surface phenology measurements from MODIS to

21   quantify the relative importance of photoperiod and thermal forcing in controlling the timing of

22   canopy greenup in eastern temperate and boreal forests of North America. The model accurately

23   predicts biogeographic and interannual variation in the timing of greenup across the study region

24   (median RMSE = 4.6 days, median bias = 0.30 days). Results reveal strong biogeographic

25   variation in the period prior to greenup when temperature and photoperiod influence greenup that

26   covaries with the importance of photoperiod versus thermal controls. Photoperiod control on leaf

27   emergence is dominant in warmer climates, but exerts only modest influence on the timing of

28   leaf emergence in colder climates. Results from models estimated using ground-based

29   observations of cloned lilac are consistent with those from remote sensing, which supports the

30   realism of remote sensing-based models. Overall, results from this study suggest that apparent

31   changes in the sensitivity of trees to temperature are modest and reflect a trade-off between

32   decreased sensitivity to temperature and increased photoperiod control, and identify a transition

33   in the relative importance of temperature versus photoperiod near the 10 ℃ isotherm in mean

34   annual temperature. This suggests that the timing of leaf emergence will continue to move earlier

as the climate warms, and that the magnitude of change will be more pronounced in colder regions with mean annual temperatures below 10 ℃.

1. Introduction

There is overwhelming evidence that leaf emergence is occurring earlier in temperate and boreal forests (Menzel et al., 2006; Schwartz et al., 2006). However, a number of recent papers have concluded that the sensitivity of leaf emergence to changes in temperature has decreased in recent decades (Fu et al., 2015; Piao et al., 2017) and that the period when trees are sensitive to thermal forcing is becoming shorter (Fu et al., 2019; Güsewell et al., 2017; Wenden et al., 2020). These results complicate interpretation of observed trends and exacerbate challenges involved in forecasting how the phenology of trees will change in the future. These challenges are further complicated by fundamental issues in the way that the sensitivity of phenological events to temperature is generally quantified (Keenan et al., 2019). Because changes in phenology impact important ecosystem functions (Keenan et al., 2014; Richardson et al., 2013), understanding how changes in climate affect phenology is critical to forecasting how ecosystems will respond to future climate change (Peñuelas et al., 2009; Piao et al., 2019).

To address this, a variety of recent studies have focused on improving understanding of bioclimatic controls on plant phenology (Liu et al., 2017; Zohner et al., 2016). Results from both lab- and field-based experimental studies have provided insights (Montgomery et al., 2020; Richardson et al., 2018a), but are limited by the fact that phenological behavior in controlled laboratory- and field-based warming experiments differs from behavior observed in natural ecosystems (Clark et al., 2014a; Wolkovich et al., 2012). Further, the manner in which environmental conditions are perturbed in such experiments (e.g., 2 ℃ warming) is not representative of climate changes expected in the future, which are predicted to occur gradually, but with large year-to-year variability (Schewe et al., 2019; Walther et al., 2002). These issues are compounded by the fact that the geographic sampling of data sets used in these studies is

63 often limited and does not reflect the full biogeographic range of species examined (Richardson

64 et al., 2013). Hence, geographic variation in the relative importance of different climate drivers

65 on phenology, both within and across plant communities, is not well understood (Piao et al.,

66 2019).

67   One widely used strategy for investigating the response of plant phenology to climate change

68 is to calibrate mechanistic models using weather data in combination with long-term records of

69 phenology collected on the ground (Basler, 2016; Fu et al., 2019) or from remote sensing (Liu et

70 al., 2017; Melaas et al., 2018). In addition to thermal controls, photoperiod is widely assumed to

71 control the timing of leaf emergence by regulating the entrance of ecodormancy, triggering

72 thermal forcing to stimulate bud swelling and leaf emergence (Chuine et al., 2016; Jackson, 2009;

73 Körner and Basler, 2010). Hence, many models include explicit representation of photoperiod

74 (e.g., Blümel and Chmielewski, 2012; Masle et al., 1989; Basler, 2016; Migliavacca et al., 2012).

75 To capture the role of thermal forcing, mechanistic models generally use aggregated bioclimatic

76 variables such as growing degree days or winter chilling as their primary inputs. However, Clark

77 et al. (2014a) have suggested that the use of such aggregated quantities is problematic because

78 values for prescribed variables required by these models (e.g., start date of forcing accumulation)

79 are not identifiable.

80   In recent years, data-driven models based on state-space representations of phenological

81 processes have been developed that overcome many of the weaknesses of both mechanistic and

82 experimental approaches (e.g., Clark et al., 2014b; Qiu et al., 2020; Senf et al., 2017;

83 Seyednasrollah et al., 2018). By modeling phenological dynamics directly from data, these

84 models avoid issues arising from misspecification of functional relationships between forcing

85 variables and processes that regulate phenological development (Clark et al., 2014b). Building on

86   this approach, here we use a data-driven spring onset model in combination with gridded weather

87   data and time series of ground-based and remotely sensed observations of spring greenup dates

88   to explore biogeographic patterns in photoperiod and thermal controls on the timing of spring

89   greenup. Specifically, we use this model to : (1) quantify the relative importance of thermal

90   forcing, photoperiod, and winter chilling in controlling spring greenup; (2) identify the pre-

91   season period when plants are sensitive to bioclimatic controls; and (3) characterize how

92   covariance among thermal forcing, photoperiod, and the length of the pre-season period control

93   the biogeography of spring greenup in deciduous forests of eastern temperate and boreal North

94   America.

95

96   **2. Methods**

97   **2.1. Study Region**

98   The study region includes the Northern Forests and Eastern Temperate Forest ecoregions

99   included in level 1 of the US EPA Ecoregions of North America (Fig. A1). To distinguish

100   deciduous forests from evergreen forests and other land cover types within the study area, the

101   500 m Collection 6 MODIS Land Cover Type product was used. This product provides annual

102   land cover maps based on machine learning that are post-processed using a multi-temporal state-

103   space modeling framework that reduces spurious land cover change introduced by classification

104   uncertainty in individual years (Abercrombie and Friedl, 2016; Sulla-Menashe et al., 2019).

105   The continuous development spring onset model (Section 2.3) is estimated on an equal-area

106   grid, where each grid cell is 4.67 km x 4.67 km (10×10 MODIS pixels; ~22 km^2). In each grid

107   cell, only pixels labeled as deciduous broadleaf or mixed forests throughout the entire study

108   period from 2001-2017 were included in the analysis. To ensure analyses were based on grid

109   cells dominated by deciduous forest cover, we excluded model grid cells where the fraction of

110   MODIS pixels labeled as deciduous broadleaf or mixed forests was less than 50% (Fig. A1).

111

112   **2.2. Spring Greenup and Meteorological Data**

113   To identify the timing of springtime leaf emergence from 2001 to 2017, we used the

114   Collection 6 MODIS Land Cover Dynamics product (MCD12Q2; Gray et al., 2019). This

115   product uses time series of the two-band Enhanced Vegetation Index (EVI2) to identify the

116   timing of six key phenophase transition dates during each growing season in each 500-m MODIS

117   pixel. Numerous studies have reported that this product provides a reliable measure of vegetation

118   phenology (Moon et al., 2019; Richardson et al., 2018b) and seasonal changes in ecological

119   function and surface biophysical characteristics (Melaas et al., 2013; Moon et al., 2020). For this

120   analysis, we use the MCD12Q2 'greenup' metric, which is defined by the Land Cover Dynamics

121   product as the day of year (DOY) during the greenup phase in spring when the EVI2 time series

122   at each pixel crosses 15% of its seasonal amplitude (Gray et al., 2019).

123   To provide the meteorological data required for model estimation, we used the Version 3

124   Daymet dataset for North America (Thornton et al., 2017) (https://daymet.ornl.gov). This data

125   set uses digital elevation data in association with a land-water mask and meteorological

126   observations collected at ground-based stations to create gridded time series of surface

127   meteorological fields at daily time step and 1 km spatial resolution for the period 1980 to present.

128   For this work, we used daily maximum and minimum 2-m air temperatures from 2000 to 2017

129   along with daylength, resampled to 500 m and co-registered to the MODIS data over all grid

130   cells included in our analysis.

131

7

2.3. Continuous Development Spring Onset Model

To estimate the sensitivity of different climatological controls on springtime phenology, we developed a continuous development spring onset model (hereafter, CDSOM) based on a hierarchical Bayesian framework that predicts the timing of springtime greenup using three drivers: photoperiod, thermal forcing, and chilling units. The original form of this model was proposed by Clark et al. (2014b), who used the same general approach to show that because conventional process-based phenology models (e.g., Hufkens et al., 2018.) aggregate daily air temperature time series into cumulative sums or mean values for each year or season, they misrepresent how thermal forcing controls the timing of phenology.

Similar to Clark et al. (2014b), the CDSOM we use here tracks the continuous response of phenological development to variation in environmental controls at daily time step. To do this, the model uses a state-space framework that includes an unobservable latent state (h), which responds continuously to environmental controls and captures ecological responses to bioclimatic forcing:

$$h_{g,s,d+1} = h_{g,s,d} + \delta h_{g,s,d} \tag{1}$$

where $h_{g,s,d}$ is the latent state for grid cell g and sample (i.e., pixel) s on day d. In this framework, $\delta h_{g,s,d}$ is the increment in h from day d to day $d + 1$, which is estimated using:

$$\delta h_{g,s,d} = \begin{cases} (X_{g,s,d} \times \beta_g)(1 - h_{g,s,d}/h_{max}), & \delta h_{g,s,d} \geq 0 \\ 0, & \delta h_{g,s,d} < 0 \end{cases} \tag{2}$$

where $X_{g,s,d}$ is a matrix of predictor variables that includes the daily mean temperature ($T_{g,s,d}$), day-length (i.e., photoperiod; $L_{g,s,d}$), and chilling units ($CU_{g,s}$; defined below) on each day, and where daily mean temperature is computed as the average of daily maximum and minimum

8

151 temperatures from Daymet in each 500 m MODIS pixel. β_g is a vector of estimated model

152 coefficients for each grid cell (g), and h_{max} is the final state value of h, which is prescribed to be

153 100. Note that: (1) even though a linear formulation is used to describe the relationship between

154 model predictors and coefficients, the model accommodates nonlinear responses in phenological

155 responses to environmental controls using an asymptotic limit for the latent state (i.e., $h_{g,s,d}/$

156 h_{max}); and (2) the latent state increment is always non-negative.

157   To convert the continuous scale of the latent state (h) into a form that identifies discrete

158 phenological events (i.e., the timing of spring greenup onset), a logit transformation is used:

$$logit(P_{g,s,d}) = \kappa + \lambda \times h_{g,s,d} \qquad (3)$$

159 where $P_{g,s,d}$ is the probability that the onset occurs at sample pixel s in grid g on day d, and κ and

160 λ are the intercept and slope of the transformation, respectively. Because greenup onset is

161 defined to be a discrete event, $P_{g,s,d}$ follows a Bernoulli distribution:

$$Y_{g,s,d} \sim Bernoulli(P_{g,s,d}) \qquad (4)$$

162 where $Y_{g,s,d}$ indicates whether or not greenup onset has occurred for sample s in grid g on day d.

163   Following convention, chilling units ($CU_{g,s}$) were defined as:

$$CU_{g,s} = \sum_{d=c_{g,0}}^{c_{g,s}} I(T_{g,s,d} < T_b) \qquad (5)$$

164 Hence, $CU_{g,s}$ is defined as the number of days below prescribed threshold T_b during the period

165 after the onset of dormancy until an unobserved date $c_{g,s}$ when the chilling requirement is

166 satisfied. Previous studies have suggested that boreal and temperate tree species respond to air

167 temperatures ranging from -5 to 10 ℃ as a threshold for chilling requirements (Hänninen et al.,

168 2019). Here we used 0 ℃ because the study area covers a large range of climate conditions.

169 Further, and more importantly, sensitivity analyses revealed that model results were not sensitive

170 to variation in T_b (not shown), which is supported by results indicating that chilling control on

171 the timing of greenup is minor (see Results).

172

173 **2.4. CDSOM Estimation**

174 As we described above, the CDSOM was estimated using a regular grid, with each grid

175 cell composed of 100 MODIS pixels. We excluded all pixels with more than one land cover type

176 label between 2001 and 2017 (i.e., that nominally experienced change) and excluded all cells that

177 were composed of less than 50% deciduous or mixed forests. Because the CDSOM is

178 computationally expensive, we used a two-stage sampling approach to estimate the model for

179 randomly selected grid cells in each of the 13 MODIS tiles that intersect the study region. In the

180 first stage, we randomly sampled grid cells within each MODIS tile that met the criteria listed

181 above. If less than 300 valid grid cells were available within a tile, we included all valid grid

182 cells. If more than 300 grid cells were available in a tile, we randomly selected a sample of 300

183 cells. In the second stage, we randomly selected MODIS pixels located in each grid cell across

184 time. To minimize the impact of spatial and temporal correlation, we used a sub-sample of 100

185 pixel-years (i.e., 100 unique greenup dates randomly selected across 17 years) to estimate a

186 unique model for each cell. Each sample was selected from a total pool of between 850-1700

187 sample points (i.e., 50-100 pixels per year in each grid across 17 years).

188 For each year, December 1st of the previous year and DOY 250 (~Sept. 7) of the current year

189 were used as the start and end dates of latent state development, respectively. Posterior sampling

190   was performed using the "R2jags" package in R (Su and Yajima, 2015), with 10,000 iterations

191   and 3,000 burn-in periods. As a final step, to reduce noise in our results, we excluded grid cells

192   where estimated model coefficients were outside 95% of the range of estimated model

193   coefficients across all grid cells. This yielded a final data set consisting of 1,685 grid cells with

194   valid results.

195

196   Model results from a representative grid cell are shown in Fig. 1. Overall, predicted onset

197   dates are well aligned with observed onset dates at this grid cell, with a root-mean-square error

198   (RMSE) of 3.7 days across the time series (Fig. 1a). Because the input forcing data are

199   normalized prior to model estimation (i.e., having a mean of 0 and a standard deviation of 1 for

200   each of the input variables in each grid g and sample s), the posterior distributions for each

201   model coefficient, which reflect the dependence of phenological development on each input

202   variable, show differences that are independent of the magnitude or units of each input variable

203   (Fig. 1b). Time series of the latent state generated by the model (Fig. 1c) provide information

204   regarding the timing and duration of the pre-season period prior to greenup onset. This period

205   has been previously described as "as the most temperature-sensitive period preceding the

206   phenological event" (Güsewell et al., 2017) or "the period before leaf unfolding for which the

207   partial correlation coefficient between leaf unfolding and air temperature is highest" (Fu et al.,

208   2015). Here we define this period as corresponding to the time interval when phenological

209   development is affected by bioclimatic forcing, and we use the CDSOM to identify the "pre-

210   season period" as starting on the DOY when the latent state variable (h) starts to increase and

211   ending on the DOY when greenup onset occurs (i.e., the period indicated by the arrow in Fig. 1c).

11
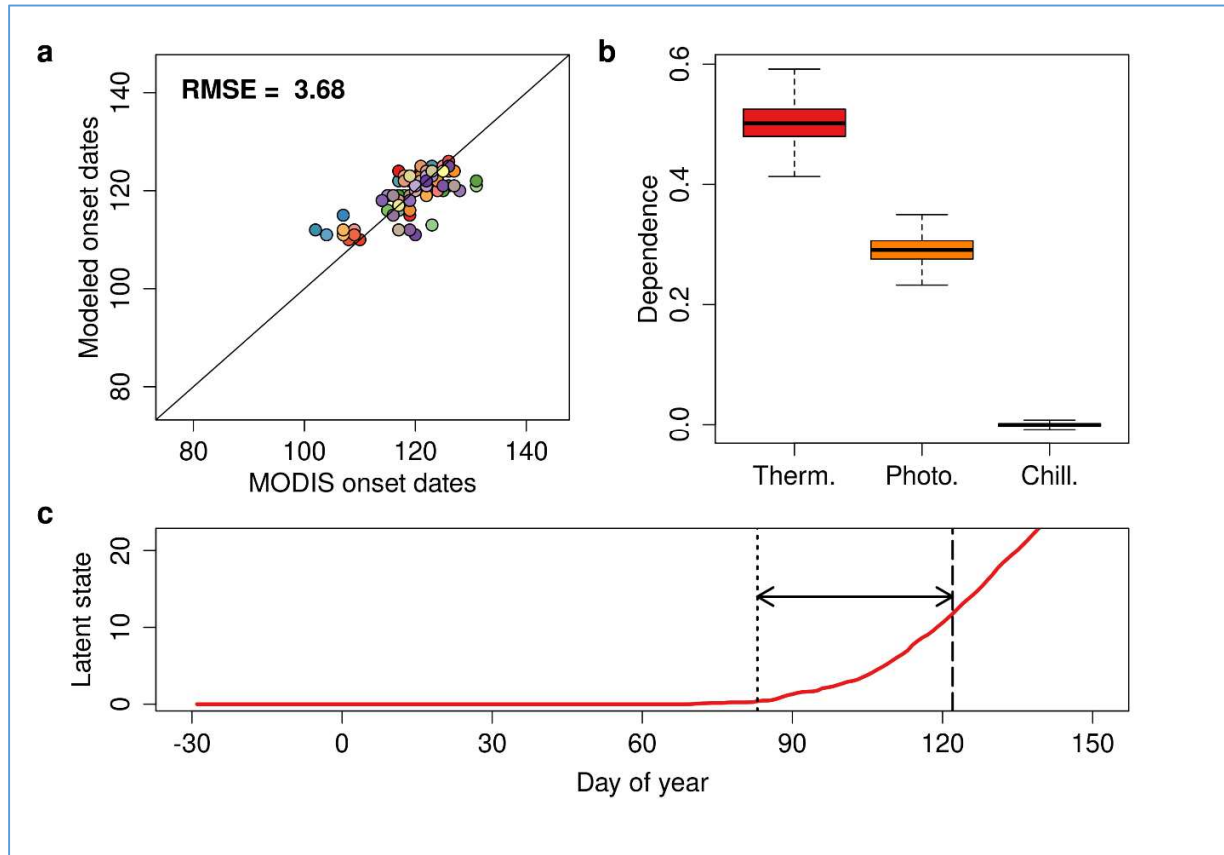
Fig. 1. Model results for a randomly selected grid cell. (a) Relationship between the greenup onset dates from MODIS and onset dates estimated by the model. (b) The distribution of model coefficients for each control variable (i.e., the relative dependence on each climate control; Therm.: thermal forcing; Photo.: photoperiod; Chill.: chilling units). (c) Time series of the latent state (red line) and the length of the pre-season (identified by the horizontal arrow). In panel (a), each dot (total n = 100) represents an individual pixel-year sampled from the grid cell comprised of 10 by 10 MODIS pixels across 17 years of the study period (i.e., 100 out of the total 1,700 pixel-years).

2.5. Quantifying the Relative Importance of Bioclimatic Forcing Variables

To address our goal of quantifying the relative importance (and geographic variation thereof) among bioclimatic controls on the timing of springtime phenology, we compute a normalized index with values that range from -1 to +1 that captures this effect. Because each of the input variables in each grid g and sample s have been normalized to have a mean of 0 and a standard deviation of 1, model coefficients can be directly compared to assess the relative importance of each control variable. To quantify this, we calculated the relative importance (RI) of each control variable relative to each other variable using a normalized index computed from CDSOM model results. For example, to compute the relative importance of photoperiod versus thermal forcing in any given grid cell, we computed:

$$RI = \frac{\beta_T - \beta_L}{\beta_T + \beta_L} \tag{6}$$

where β_T and β_L are the average model coefficients for thermal forcing and photoperiod (respectively) during the pre-season period, which are estimated for each grid cell by the CDSOM.

2.6. CDSOM Assessment and Comparison with Conventional Phenology Models

To provide a baseline comparison against previously developed and widely used springtime phenology models (hereafter, the 'conventional models'), we compared results from the CDSOM with four widely used process-based phenology models included in the "phenor" package in R (Hufkens et al., 2018). Specifically, we compared our results against the thermal time (TT) model, the photo-thermal time (PTT) model, the exponential photo-thermal time model (M1), and the alternating (AT) model, as described by Hufkens et al. (2018). These models are

13

243 fundamentally different from the CDSOM in that they assume a linear relationship between

244 spring thermal forcing and the rate of phenological development, and that spring onset occurs

245 when accumulated forcing (after a prescribed start date) reaches a critical threshold (F^*). The TT

246 model relies only on thermal forcing (daily air temperature in each MODIS pixel, $T_{g,s,d}$) with no

247 additional inputs. In this model, the state of forcing (S_f) increases each day until F^* is reached,

248 when leaves emerge (Chuine et al., 1999; Hunter and Lechowicz, 1992):

$$R(T_{g,s,d}) = \begin{cases} 0 & for\ T_{g,s,d} \le T_b \\ T_{g,s,d} - T_b & for\ T_{g,s,d} \ge T_b \end{cases} \qquad (6)$$

$$S_f = \sum_{t_0}^{t} R(T_{g,s,d}) \qquad (7)$$

249 where t_0 is the starte date. For consistency with the CDSOM, we set t_0 and T_b to December 1st

250 and 0 °C, respectively. The PTT model includes day-length (i.e., photoperiod; $L_{g,s,d}$) as an

251 additional factor that regulates the rate of thermal forcing (Črepinšek et al., 2006; Masle et al.,

252 1989):

$$S_f = \sum_{t_0}^{t} R(T_{g,s,d}) \times \frac{L_{g,s,d}}{24} \qquad (8)$$

253 The exponential M1 model also includes photoperiod, but treats the relationship between

254 photoperiod and S_f as an exponential (Blümel and Chmielewski, 2012):

$$S_f = \sum_{t_0}^{t} R(T_{g,s,d}) \times \left(\frac{L_{g,s,d}}{24}\right)^k \qquad (9)$$

255 where k is an empirically estimated constant. Finally, the AT model includes the number of days

256 when the daily mean temperature falls below T_b (i.e., the number of chilling days; NCD), and

14

257   treats NCD as an exponential function that reduces the thermal forcing accumulation required for

258   spring onset to occur (Cannell and Smith, 1983):

$$F^* = a + b \times \exp[c \times \text{NCD}(t)] \tag{10}$$

259   where a, b, and c are empirically estimated constants, and $\text{NCD}(t)$ is defined as the number of

260   chilling days since December 1st. A table summarizing the variables and main characteristics of

261   the CDSOM and conventional models is provided as an appendix (Table A1).

262   For this analysis, we assessed model performance for both the CDSOM and the conventional

263   models in two ways. First, we assessed results from model-based predictions for the timing of

264   spring greenup based on all available years (from 2001 to 2017). Second, to provide a more

265   robust   assessment of model performance, we held out two years (2010 and 2012) with

266   anomalously warm springs in much of the study region (Friedl et al., 2014), and evaluated model

267   performance for each of these years. In this way, we were able to assess not only how well the

268   models performed under average conditions, but also how well they performed under unusual

269   springtime weather conditions that were not represented in the data used to estimate the models.

270

271   **2.7. CDSOM Estimation Using Ground-Based Observations**

272   As a final element of our analysis, to complement model results based on remotely sensed

273   greenup dates and to provide an independent basis for assessing the realism and robustness of

274   our results, we estimated the CDSOM using time series of leaf unfolding dates for cloned lilac

275   (*Syringa x chinensis* 'Red Rothomagensis') (Rosemartin et al., 2015). By applying the model to

276   data from cloned plants, genetic variability is eliminated, and which allows us to investigate how

277   differences in the timing of leaf unfolding between different individuals are caused by

15

278   differences in local environmental controls. Unlike our approach using MODIS spring greenup

279   dates, the model is estimated by pooling site-years across the region because the number of lilac

280   leaf-out dates for each location is too small to accurately estimate models for each site. The

281   dataset includes 254 leaf unfolding dates from 60 locations across the study region, spanning the

282   period from 2001 to 2008 (Fig. A1). For reasons we explain below, we stratified the dataset into

283   'warm' versus 'cold' sites based on whether the mean annual temperature at each site is above or

284   below 10 ℃. Based on this stratification, the model was applied to 182 and 72 leaf unfolding

285   dates for the colder and warmer regions, respectively.

286

287   **3. Results**

288   The CDSOM accurately predicts biogeographic and interannual variation in the timing of

289   springtime greenup across the study region. The median RMSE between predicted and observed

290   spring greenup dates was 4.6 days (Fig. 2), which is roughly equivalent to the uncertainty in

291   spring greenup dates estimated from MODIS (Moon et al., 2019). Inspection of results from the

292   conventional spring onset models show that median RMSEs were ~20% larger (~5.5 days vs. 4.6

293   days) relative to those obtained from the CDSOM (Fig. 2b). Further, RMSEs for years with

294   anomalous springs (2010 and 2012) were unchanged for the CDSOM, but increased by roughly 2

295   days for conventional models when 2010 and 2012 were excluded during model estimation (Fig.

296   3). For completeness, Fig. A2 shows the relationship between anomalies in MODIS greenup

297   dates and anomalies in predicted onset set dates, and demonstrates that the CDSOM outperforms

298   the conventional models in capturing year-to-year variations in spring onset dates. These results

299   suggest that the CDSOM not only provides more accurate predictions of greenup relative to

300   predictions from conventional phenology models, but that the CDSOM more effectively captures

301   the impact of geographic and year-to-year variation in bioclimatic controls. More generally, the

302   accuracy of CDSOM results indicates that the model realistically captures the nature and

303   magnitude of ecophysiological responses to interannual and biogeographic variation in climate

304   controls that regulate the timing of greenup.

305
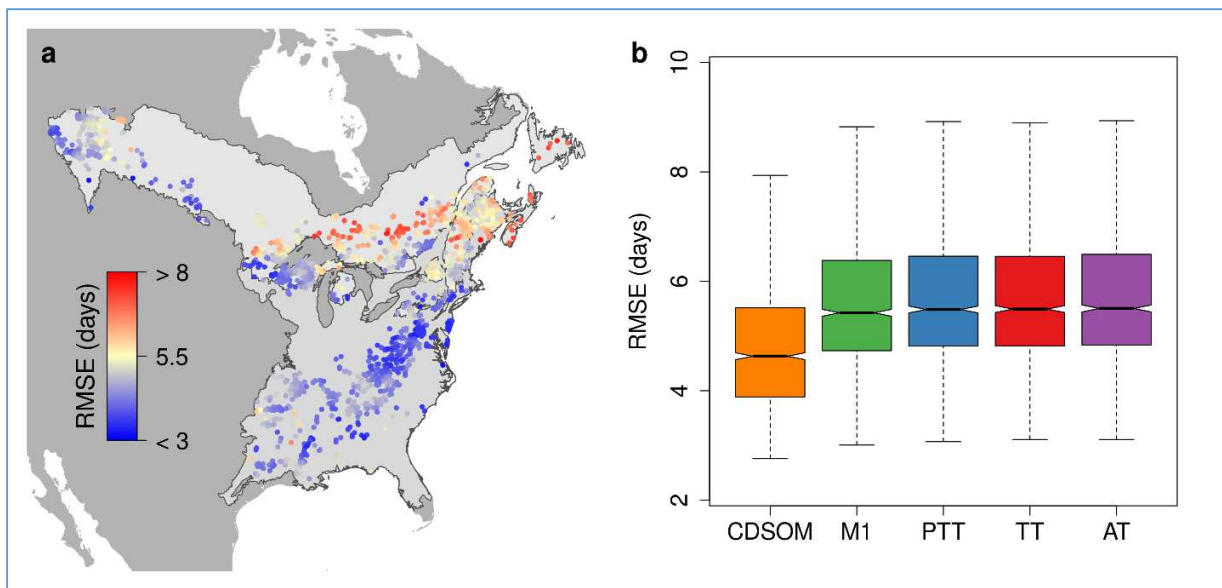
306

307   **Fig. 2.** Continuous Development Spring Onset Model (CDSOM) performance. (a) Geographic

308   variation in model root-mean-square error (RMSE) between greenup onset dates observed from

309   MODIS and onset dates predicted by the CDSOM model. (b) Boxplots showing the distribution

310   of RMSEs for the CDSOM model and four widely used conventional spring greenup models.

311   M1: The exponential photo-thermal time model; PTT: The photo-thermal time model; TT: The

312   thermal time model; AT: The alternating model. In panel (b), boxplots are presented in

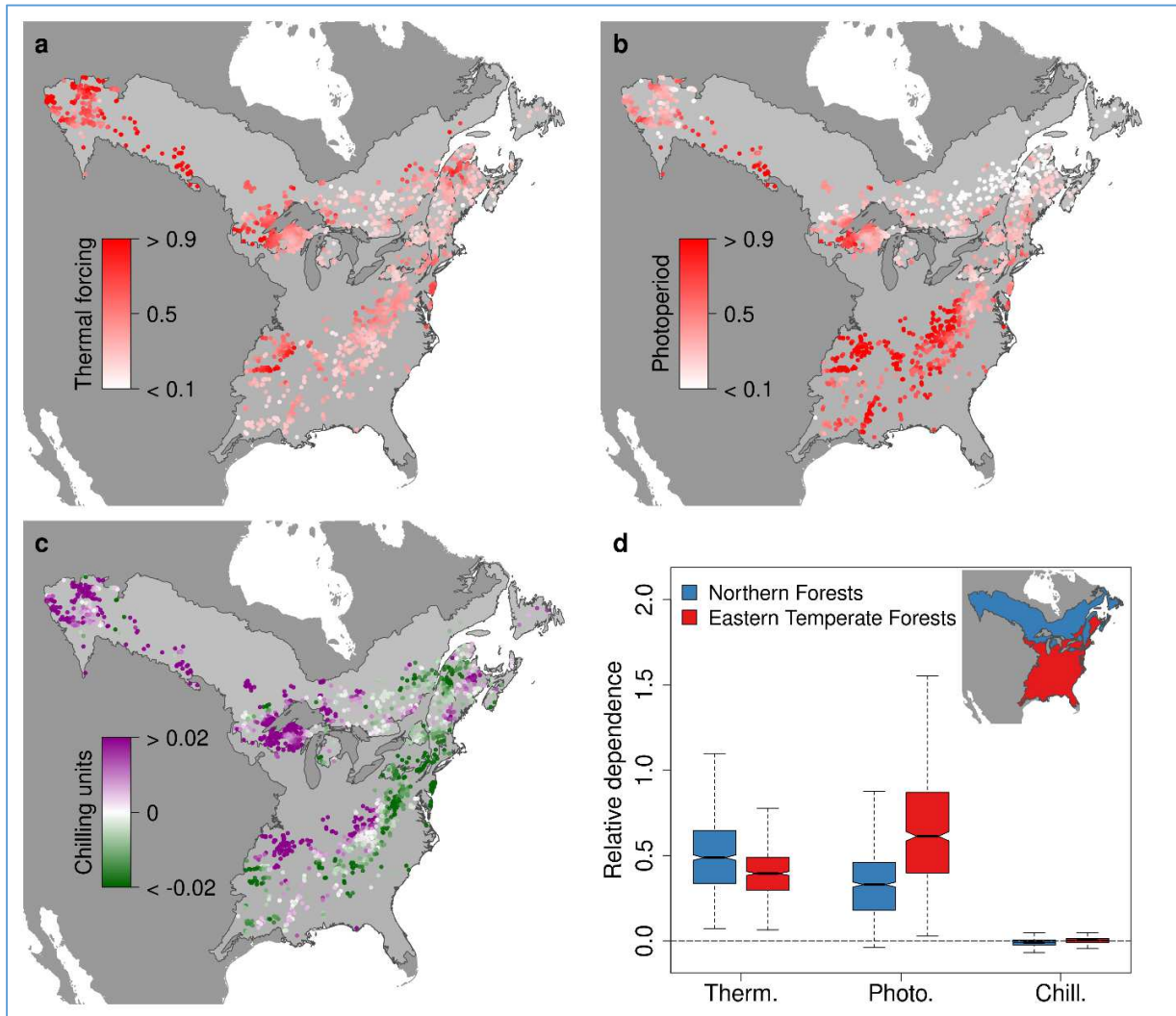313   increasing order of magnitude with respect to mean RMSE.

314

315
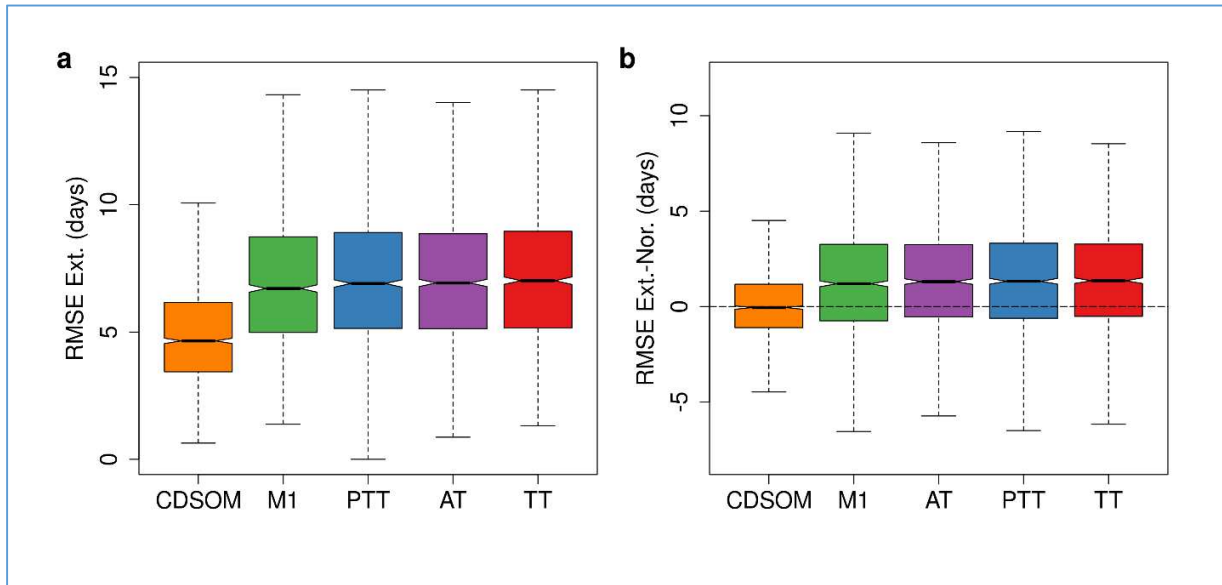
17

Fig. 3. RMSE results across models for anomalous years. (a) Boxplots of RMSEs for each model for 2010 and 2012. (b) Boxplots showing increase in RMSEs for model predictions for all years versus anomalous years (i.e., RMSEs for 2010 and 2012 – RMSEs for 2001-2017) at each grid cell. CDSOM: continuous development spring onset model; M1: The exponential photo-thermal time model; PTT: The photo-thermal time model; TT: The thermal time model; AT: The alternating model. Boxplots are presented in increasing order of magnitude with respect to mean RMSE.

326

Fig. 4. Geographic variation in the dependence of spring greenup onset date to: (a) thermal forcing, (b) photoperiod, and (c) chilling units. In panel (d), boxplots show the distribution of model coefficients for each control variable during the pre-season period prior to leaf emergence in Northern Forests (blue) versus Eastern Temperate Forests (red). Differences between the means in both cases are statistically significant ($p < 0.001$).

332

333   The dependence of spring greenup on thermal forcing estimated by the CDSOM is higher in

334   Northern Forests than in Eastern Temperate forests (Fig. 4), but overall differences, while

335   statistically significant, are modest. In contrast, dependence on photoperiod control exhibits

336   systematic geographic variation across the study domain, with large differences between each

337   ecoregion. Eastern Temperate Forests, which are warmer, show substantially higher dependence

338   on photoperiod relative to the Northern Forests ecoregion, which is much cooler (Fig. 4b and 4d).

339   This difference is especially pronounced in Eastern Canada where dependence on photoperiod is

340   low, versus the Southern United States, where photoperiod dependence is high. Dependence of

341   spring onset on chilling units is uniformly low throughout the study region, which indicates that

342   the influence of chilling control, relative to photoperiod and thermal forcing, is effectively

343   negligible (Fig. 4c and 4d).

344   Geographic patterns in the *RI* of photoperiod versus thermal forcing indicates that

345   photoperiod exerts proportionally more control on the timing of spring greenup in warmer

346   regions, while thermal forcing exerts proportionally more control in colder regions (Fig. 5a). By

347   plotting the *RI* in climate space (i.e., as a function of mean annual temperature and precipitation)

348   (Fig. 5b), the pattern becomes even more clear. In regions where mean annual temperature is

349   above ~10 ℃, photoperiod exerts stronger control on the timing of spring greenup than thermal

350   forcing. Conversely, in regions where mean annual temperature is less than ~10 ℃, thermal

351   forcing is more important. *RI* values near the 10 ℃ isotherm in mean annual temperature are

352   generally close to zero, indicating equal influence of thermal forcing and photoperiod (plotted as

353   purple points in Fig. 5). These results suggest that the 10 ℃ isotherm in mean annual

354   temperature identifies a transition zone between regions where thermal forcing versus

355   photoperiod is more dominant.
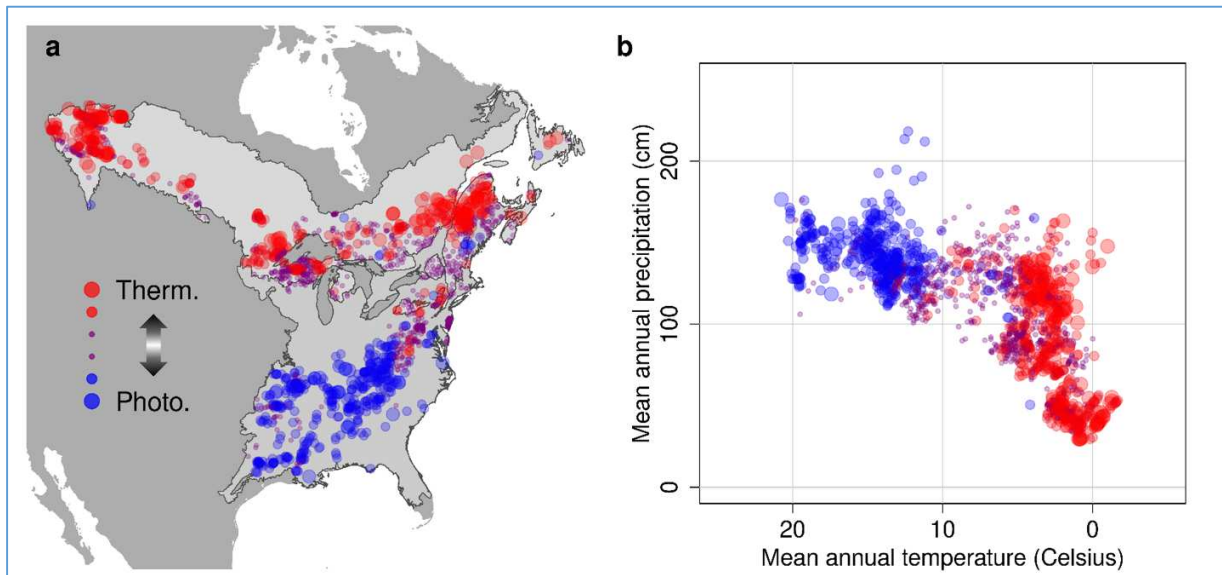
Fig. 5. Relative importance (*RI*) of thermal forcing versus photoperiod. Circles in red and blue show locations where thermal forcing and photoperiod, respectively, exert stronger control on the timing of spring greenup; purple circles identify locations where the magnitude of thermal forcing and photoperiod are roughly equivalent. The size of each circle is proportional to the magnitude of *RI* in each cell.

Results from applying CDSOM to ground-based observations of leaf unfolding dates for cloned lilac reveal that even though the individual lilac plants are genetically identical, the relative dependence of leaf unfolding dates on thermal forcing versus photoperiod depends on local bioclimatic conditions (Fig. 6). Consistent with previous studies (Basler and Körner, 2012; Schwartz et al., 2006), model coefficients and *RI* values indicate that leaf unfolding in cloned lilac depends more strongly on thermal forcing than on photoperiod, irrespective of location. However, thermal control is stronger in colder regions and *RI* values are significantly smaller

371 (i.e., thermal control is less dominant) in warm sites than in cold sites. In addition, comparison of

372 cloned lilac data against greenup dates from MODIS for the same location show that MODIS

373 greenup dates are biased late relative to lilac unfolding dates (Fig. A3), especially in warmer

374 areas with earlier greenup dates, which supports the conclusion that lilacs are sensitive to

375 temperature.

376
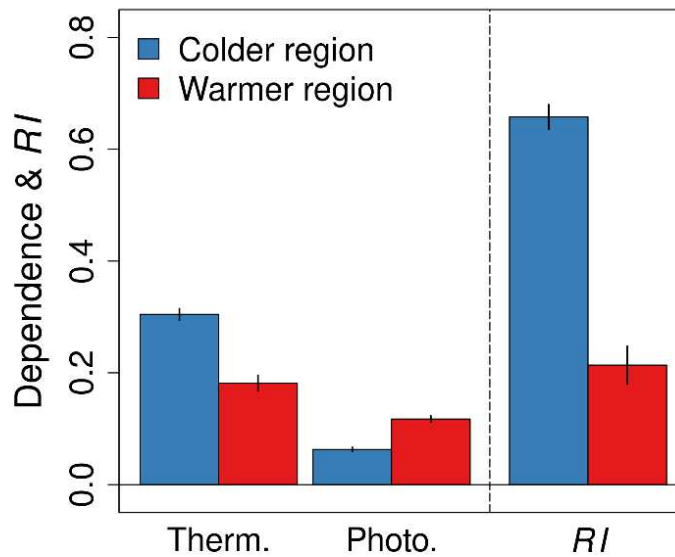
377

378 **Fig. 6.** Dependence of cloned lilac leaf unfolding date on thermal forcing and photoperiod, and

379 relative importance (*RI*). 254 total leaf unfolding dates from cloned lilac were divided into two

380 groups based on mean annual temperature (≤ 10 ºC, $n = 182$; > 10 ºC, $n = 72$). The left panel

381 plots the mean dependence of leaf unfolding on thermal forcing and photoperiod estimated by

382 the CDSOM. The right panel plots the mean *RI* in each group. Positive *RI* indicates stronger

383 control by thermal forcing relative to photoperiod. Vertical lines show ±1 standard deviation.

384

385   Finally, results from the CDSOM reveal patterns of covariance among pre-season period

386   length, photoperiod, and thermal forcing that jointly control the timing of greenup that are not

387   captured in conventional models. In particular, geographic variation in the pre-season period is

388   strongly and negatively correlated with geographic variation in the relative importance of

389   photoperiod on spring greenup. Fig. 7b shows that this relationship follows a power law, where

390   photoperiod control decreases (R^2 = 0.70, p < 0.001) as the length of the pre-season period

391   increases. Fig. 7b also reveals modest heteroscedasticity in the relationship between pre-season

392   period length and photoperiod control, which reflects the fact that spring greenup in locations

393   with cooler mean annual temperatures and longer pre-seasons have lower dependence on

394   photoperiod and higher dependence on thermal forcing (Fig. 5). In contrast, the relationship

395   between pre-season period and dependence on thermal forcing is statistically significant, but

396   much weaker (R^2 = 0.13; Fig. A4).

397
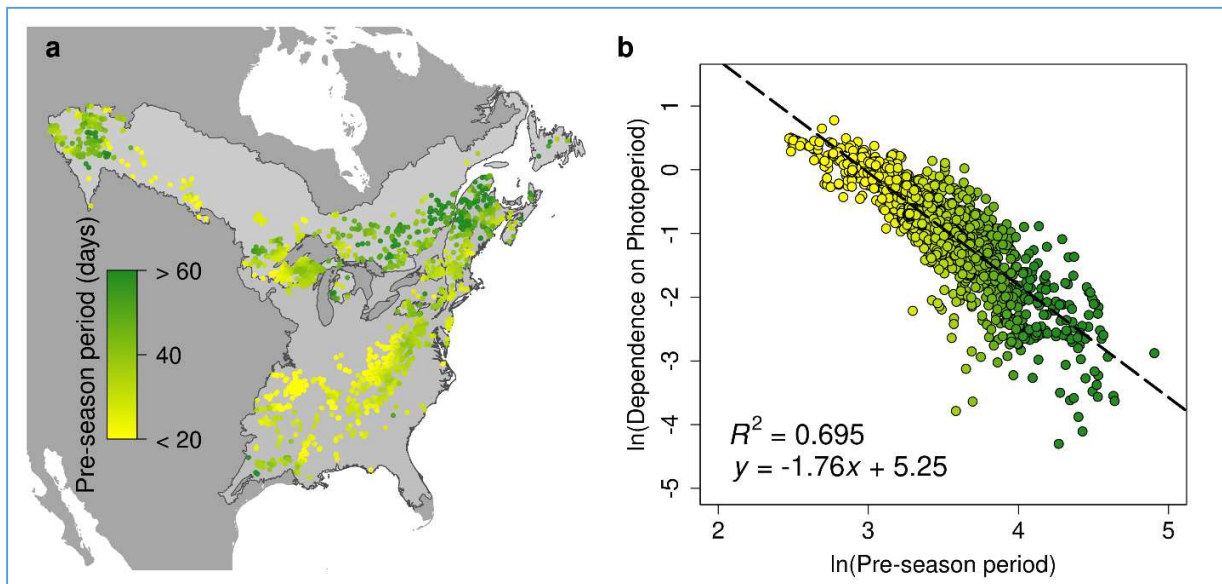
398

399 **Fig. 7.** Variation in pre-season period and the relationship between greenup dependence on

400 photoperiod and length of pre-season period. (a) Geographic pattern in pre-season period, and (b)

401 log-log relationship between the dependence of greenup on photoperiod and the length of the

402 pre-season period.

403

404 **4. Discussion**

405   We assessed the relative importance of photoperiod, chilling, and thermal forcing in

406 controlling the timing of leaf emergence in Eastern Temperate and Boreal Forest ecoregions of

407 North America. To do this, we used a hierarchical Bayesian model in combination with time

408 series of land surface phenology measurements from remote sensing. The former provides a

409 data-driven framework for investigating how different bioclimatic controls influence the timing

410 of leaf emergence (Clark et al., 2014b; Seyednasrollah et al., 2020); the latter provides a robust

411 and repeatable means of measuring and monitoring phenological dynamics over large areas

412 (Bolton et al., 2020; Zhang et al., 2018).

413   The core hypotheses that motivate this research include two main elements. First, the

414 ecophysiological processes that control leaf emergence respond continuously to variation in

415 environmental controls throughout pre-season period prior to greenup in a manner that is not

416 represented in conventional models (Clark et al., 2014b). Second, rather than simply acting as a

417 cue for entering ecodormancy, photoperiod exerts continuous control on the timing of greenup

418 during the pre-season period. The results presented in this study suggest that both hypotheses are

419 supported. The preseason period, which corresponds to the period when the CDSOM latent state

420 variable (h) responds to bioclimatic forcing (Fig. 1c), ranges from roughly 2-12 weeks over the

421 study domain (Fig. 7a). Throughout this period, changes in h reflect the net effect of daily

24

422 changes thermal and photoperiod controls. By estimating the model in a spatially explicit fashion

423 over a large geographic and climatic range, CDSOM results provide an empirical basis for

424 quantifying not only how thermal forcing and photoperiod individually and jointly influence the

425 timing of greenup, but more generally, how the length of the preseason period and relative

426 importance of photoperiod versus thermal forcing vary over the study domain.

427 Conventional models calibrated using long-term observations of phenological events such as

428 those used in this study have been widely used to simulate and forecast phenological events for

429 decades (Chuine and Régnière, 2017). Like the CDSOM, these models generally use air

430 temperature, photoperiod, and chilling units in different configurations and combinations to

431 parameterize the response of plants to bioclimatic controls and predict the timing of phenophase

432 transitions (Basler, 2016; Hufkens et al., 2018). However, as we described previously, Clark et al.

433 (2014a, 2014b) argue that most conventional phenology models are fundamentally limited

434 because: (1) they aggregate measurements with substantial day-to-day variability over periods of

435 weeks-to-months into single parameters and therefore do not capture how short-term variability

436 in control variables influences the timing of leaf emergence; (2) they rely on parameters that are

437 not identifiable; and (3) they do not account for uncertainty in model predictors or leaf

438 emergence data. As a solution, Hänninen et al. (2019) argue that carefully designed factorial

439 experiments provide the most robust basis for improving understanding of processes that control

440 leaf emergence, and hence, for developing and testing process-based models. However,

441 implementing such studies is difficult and expensive, and collecting sufficient sample data to

442 support robust and generalizable models is generally not possible. Reflecting these challenges,

443 results from a meta-analysis of warming studies showed that phenological changes observed in

25

444   such experiments do not replicate the magnitude of phenological responses to natural variation in

445   air temperature observed in natural systems (Wolkovich et al., 2012).

446   Data-driven models like the CDSOM are not a panacea, but they do resolve several of the

447   issues discussed above. In addition to addressing the three limitations identified by Clark et al.

448   (2014a, 2014b), functional relationships among control variables in CDSOM are entirely

449   estimated from data. Hence the CDSOM avoids issues related to misspecification of functional

450   relationships that are inherent to conventional models. Further, by exploiting time series of

451   remote sensing observations collected over large areas that span nearly two decades, the

452   CDSOM results presented here capture and reflect a much broader range of climate regimes and

453   climate variability than is generally possible using designed experiments. Indeed, we posit that

454   natural variability captured through interannual variability in climate over large geographic

455   scales provides an important and useful strategy for characterizing and understanding the

456   sensitivity of plant phenology to climate change (Friedl et al., 2014).

457   Moreover, and perhaps most importantly, while the patterns presented in Figs. 4-7 are

458   superficially consistent with results from previous studies suggesting that the timing of spring

459   greenup in deciduous forests has become less sensitive to thermal forcing and that the so-called

460   'temperature sensitive period' of temperate and boreal trees is changing (Fu et al., 2019, 2015;

461   Piao et al., 2017). We suggest that this inference may be spurious. Specifically, results from the

462   CDSOM show that thermal forcing control on the timing of greenup is heterogeneous and

463   exhibits weak covariance with pre-season period. Hence, apparent decreases in temperature

464   sensitivity actually reflect shorter pre-season periods with increased photoperiod control (Keenan

465   et al., 2019). Stated another way, as the climate warms, higher temperatures tend to increase the

466   relative importance of photoperiod, while dependence on temperature has remained relatively

467 constant. Further, in regions where mean annual temperature is below ~10 ℃, which

468 encompasses a significant proportion of the temperate zone and all of the boreal zone,

469 photoperiod control is modest and thermal forcing is clearly the dominant control. Indeed, our

470 results suggest that the biogeographic range in which the relative importance of photoperiod

471 control is increasing is restricted to locations with mean annual temperatures between ~8-10 ℃,

472 and hence, is relatively narrow.

473   The simplest explanation for why photoperiod control varies geographically is provided by

474 the "law of the minimum", which states that plant growth is controlled by the scarcest resource

475 rather than by the total resources available (Liebig et al., 1841). Our results are, to a first order,

476 consistent with this law. In cold regions (i.e., identified here as regions where mean annual

477 temperature is less than ~10 ℃; Fig. 5), temperature is the primary limiting factor that controls

478 the timing of greenup. In warmer regions where temperature is less limiting, light (or moisture)

479 becomes the primary limiting resource. Invoking a similar argument, Park et al. (2019) suggest

480 that extensive areas of high-latitude ecosystems that were previously constrained by temperature

481 are becoming more sensitive to photoperiod. Further, the results from our study are consistent

482 with recent experimental results from Zohner et al. (2016), who concluded that springtime

483 phenology in deciduous trees at lower latitudes tended to depend more strongly on photoperiod,

484 while species at high latitudes leafed out independent of photoperiod. Hence our results are

485 consistent with both long-established and more recent ecological literature.

486   Lastly, it is important to note several limitations of the current study. First, rather than

487 modeling the role of chilling in controlling spring greenup using continuous (i.e., daily) forcing

488 (Hänninen et al., 2019; Murray et al., 1989), the CDSOM uses chilling units, which provide an

489 accumulated measure chilling requirements. This suggests that the role of the chilling units may

490   not be fully accounted for in this study, and may explain the relatively minor role of chilling

491   units in predicting the timing of spring greenup that we observed in this study (Fig. 4c and d)

492   (c.f., Heide and Prestrud, 2005; Laube et al., 2014). Second, to capture the effect of thermal

493   forcing, the CDSOM used daily mean temperature as opposed to other measures of thermal

494   forcing such as daily maximum and minimum temperature, which some studies have suggested

495   may be better predictors. However, results from CDSOM using daily maximum and minimum

496   temperatures as inputs did not show significant differences from results based on daily mean

497   temperatures (not shown), and more generally, results from studies that have explored this

498   question are somewhat inconsistent (c.f., Huang et al., 2020; Piao et al., 2015; Shen et al., 2018).

499   That said, because continuous development models are explicitly designed to capture the effects

500   of short-term variability in forcing variables, selection of optimal metrics to this variability is

501   clearly important and merits more investigation.

502

503   **5. Conclusions**

504   Changes in springtime phenology are among the most obvious and observable responses of

505   organisms to climate change, but the mechanisms behind these changes are poorly understood

506   (Parmesan and Yohe, 2003; Piao et al., 2019). By directly estimating and mapping the

507   geographic dependence of greenup on photoperiod and thermal forcing, results from this study

508   elucidate how the nature and magnitude bioclimatic control on spring phenology depend on

509   geography and climate, and provide a novel and nuanced explanation for why the temperature

510   sensitivity of deciduous forests appears to be decreasing. Specifically, our results indicate that

511   apparent changes in temperature sensitivity may reflect a misinterpretation of the data, and where

512   present, observed decreases actually reflect increased dependence on photoperiod. The results

28

513 also help to clarify the mechanisms behind observed changes and have important implications

514 for a variety of ecological processes, such as the role of safety mechanisms that are widely

515 ascribed to photoperiod constraints on spring phenology (Körner and Basler, 2010). For example,

516 Fig. 5 shows that the relative importance of photoperiod decreases as mean annual temperature

517 decreases, which suggests that safety mechanisms related to photoperiod provide only modest

518 protection in colder climates (Richardson et al., 2018a). More generally, our results support the

519 argument posited by Zohner et al. (2016) who reported that tree species with strong photoperiod

520 control on leaf-out tend to be located in warmer regions, and challenge the idea that photoperiod

521 provides a safeguard against early leaf emergence in temperate woody species.

522

527

528 **Author contributions**

529   M.M. and M.A.F designed the analysis and led the drafting of the manuscript. M.M. and B.S.

530 developed the model. MM. performed the analysis. B.S. and A.D.R. contributed analysis ideas

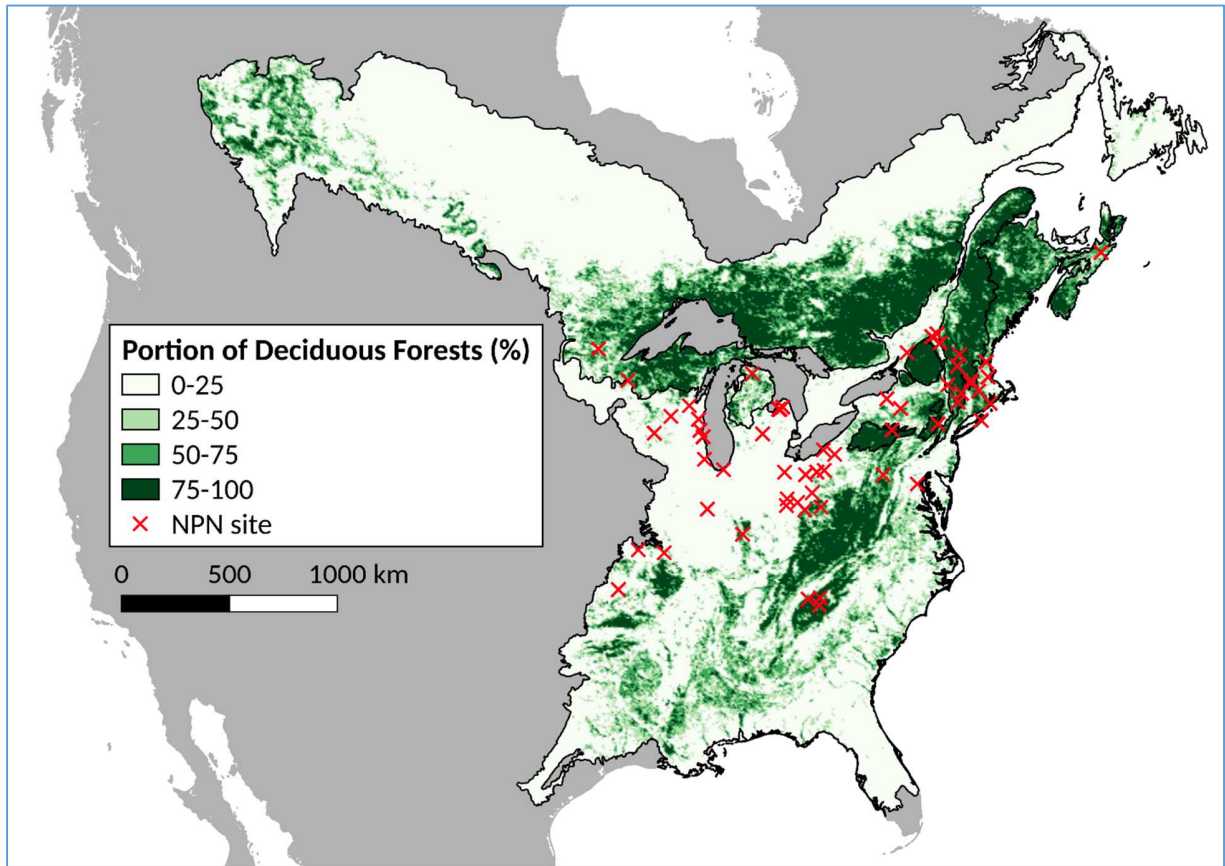531 and participated in drafting the manuscript.

532

533 **Competing interests**

534   The authors declare no competing interests.

535 **Appendix**

536 **Table A1.** Models descriptions

Model	Model type	Variables	Main characteristics & Statistical assumptions of the model
CDSOM	Date-driven	h; δh; h_{max}; X; T; L; CU; β; P; κ; λ; Y; T_b	Phenological development responses continuously to variations in environmental controls at daily time step throughout pre-season period; Invoking no assumptions about functional relationships between control variables
TT	Knowledge-driven	F^*; S_f; T; T_b	Greenup onset occurs when accumulated forcing reaches a critical threshold, which sorely relies only on thermal forcing with no additional factors
PTT	Knowledge-driven	F^*; S_f; T; T_b; L	Greenup onset occurs when accumulated forcing reaches a critical threshold, but the rate of thermal forcing is regulated by photoperiod
M1	Knowledge-driven	F^*; S_f; T; T_b; L; k	Greenup onset occurs when accumulated forcing reaches a critical threshold, but the rate of thermal forcing is regulated by photoperiod as an exponential
AT	Knowledge-driven	F^*; NCD; a; b; c	Greenup onset occurs when accumulated forcing reaches a critical threshold, but the rate of thermal forcing is regulated by the number of chilling days

537 CDSOM: Continuous Development Spring Onset Model; TT: Thermal Time model (TT); PTT: Photo-Thermal Time model (PTT);

538 M1: Exponential Photo-Thermal Time model (M1); AT: Alternating model; h: latent state; δh: daily latent state increment; h_{max}:

539 theoretical final state of h; X: matrix of predictor variables T, L, and CU (daily mean temperature, day-length, and chilling units,

540 respectively); β: vector of estimated model coefficient for T, L, and CU; P: probability that greenup onset occurs; κ and λ: intercept

541 and slope for logit transformation, respectively; Y: Bernoulli trial indicating whether or not greenup onset has occurred; T_b: base

542 temperature for chilling requirement; F^*: critical threshold that spring greenup onset occurs when the state of forcing (S_f) reaches it; k:

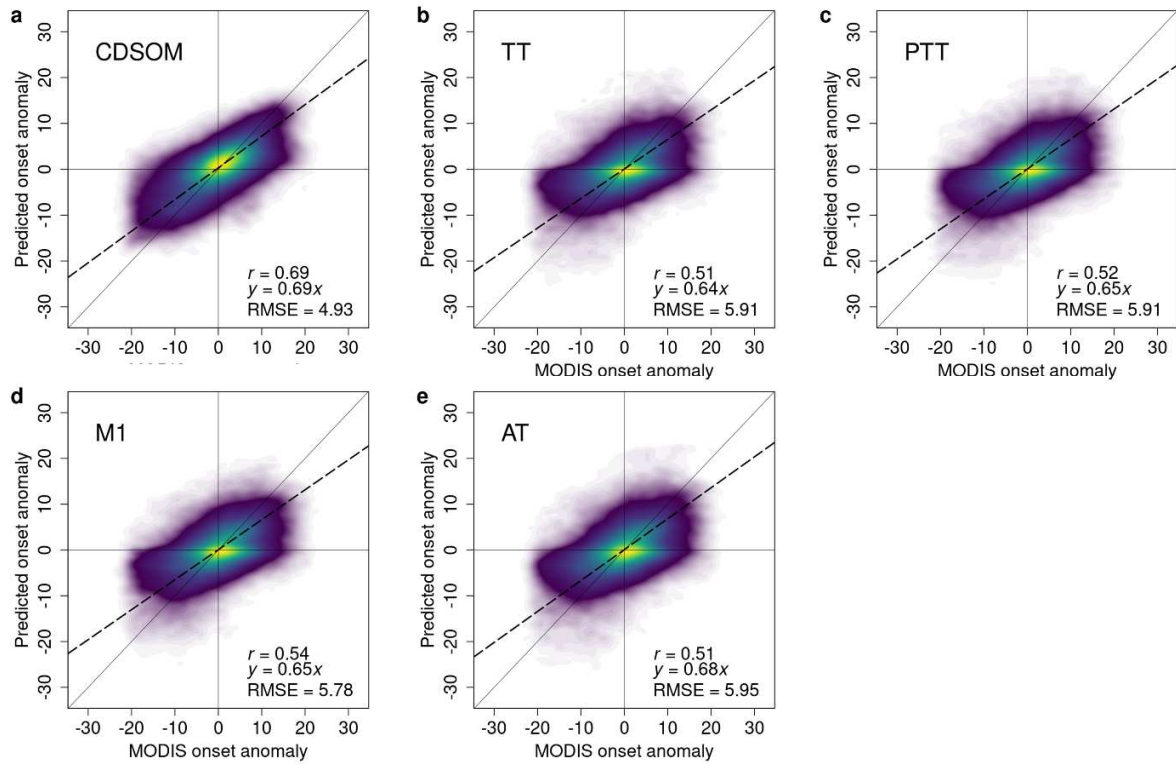543 exponential coefficient for M1; NCD: number of chilling days; estimated constants for AT

544

545

Fig. A1. Map of the study area. Extents of the US EPA Northern Forest and Eastern Temperate Forest ecoregions, along with the proportion 500 m MODIS pixels labeled as deciduous forests in each grid cell according to the Collection 6 MODIS Land Cover Type product. Red crosses show the USA-National Phenology Network site locations where lilac data are collected. Note that because the MODIS Land Cover Type product uses a threshold of 60% cover to define forest classes, the map shown in Fig. A1 modestly over-represents the actual proportion of deciduous forest cover.

553

554

Fig. A2. Relationship between anomalies in MODIS onset dates and anomalies in model-predicted onset dates. Panels (a)-(e) show results for the Continuous Development Spring Onset Model (CDSOM), the thermal time model (TT), the photo-thermal time model (PTT), the exponential photo-thermal time model (M1), and the alternating model (AT), respectively. Dashed lines and correlation coefficients (*r*) show the results from standard major axis regression.

560
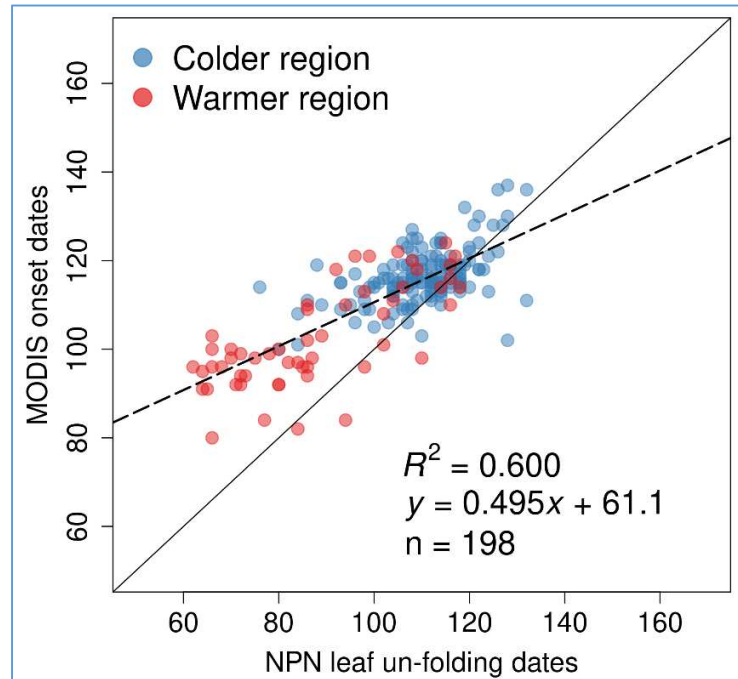
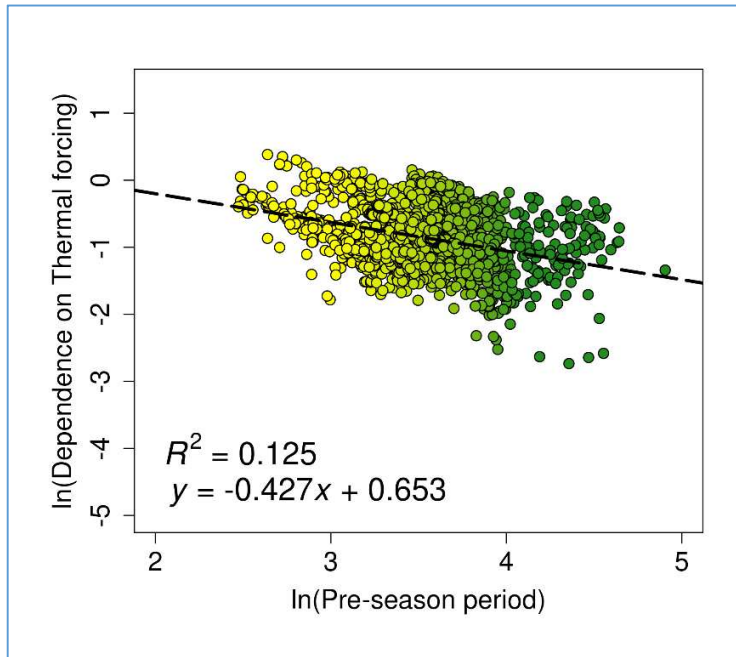**Fig. A3.** Relationship between MODIS greenup dates and leaf unfolding dates from the USA-NPN cloned lilac dataset. The colder (red dots) and warmer (blue dots) sites are divided based on mean annual temperature (i.e., colder ≤ 10 ℃; warmer > 10 ℃). *n* (= 198) is different from the total number of USA-NPN leaf unfolding dates (n = 254) due to cases where no MODIS dates were available because the lilac site was not located in a location dominated by deciduous or mixed forest at the scale of MODIS pixels.

33

The figure shows a scatter plot with x-axis labeled "ln(Pre-season period)" ranging from 2 to 5, and y-axis labeled "ln(Dependence on Thermal forcing)" ranging from -5 to 1. A dashed trend line is shown with the following statistics displayed:

$R^2 = 0.125$

$y = -0.427x + 0.653$

569

Fig. A4. Relationship between pre-season period length and dependence on thermal forcing.

571

572   **References**

573   Abercrombie, S.P., Friedl, M.A., 2016. Improving the Consistency of Multitemporal Land Cover Maps
574   Using a Hidden Markov Model. IEEE Transactions on Geoscience and Remote Sensing 54, 703–
575   713. https://doi.org/10.1109/TGRS.2015.2463689
576   Basler, D., 2016. Evaluating phenological models for the prediction of leaf-out dates in six temperate tree
577   species across central Europe. Agricultural and Forest Meteorology 217, 10–21.
578   https://doi.org/10.1016/j.agrformet.2015.11.007
579   Basler, D., Körner, C., 2012. Photoperiod sensitivity of bud burst in 14 temperate forest tree species.
580   Agricultural and Forest Meteorology 165, 73–81. https://doi.org/10.1016/j.agrformet.2012.06.001
581   Blümel, K., Chmielewski, F.-M., 2012. Shortcomings of classical phenological forcing models and a way
582   to overcome them. Agricultural and Forest Meteorology 164, 10–19.
583   https://doi.org/10.1016/j.agrformet.2012.05.001
584   Bolton, D.K., Gray, J.M., Melaas, E.K., Moon, M., Eklundh, L., Friedl, M.A., 2020. Continental-scale
585   land surface phenology from harmonized Landsat 8 and Sentinel-2 imagery. Remote Sensing of
586   Environment 240, 111685. https://doi.org/10.1016/j.rse.2020.111685
587   Cannell, M.G.R., Smith, R.I., 1983. Thermal Time, Chill Days and Prediction of Budburst in Picea
588   sitchensis. Journal of Applied Ecology 20, 951–963. https://doi.org/10.2307/2403139
589   Chuine, I., Bonhomme, M., Legave, J.-M., García de Cortázar-Atauri, I., Charrier, G., Lacointe, A.,
590   Améglio, T., 2016. Can phenological models predict tree phenology accurately in the future? The
591   unrevealed hurdle of endodormancy break. Glob Change Biol 22, 3444–3460.
592   https://doi.org/10.1111/gcb.13383
593   Chuine, I., Cour, P., Rousseau, D.D., 1999. Selecting models to predict the timing of flowering of
594   temperate trees: implications for tree phenology modelling. Plant, Cell & Environment 22, 1–13.
595   https://doi.org/10.1046/j.1365-3040.1999.00395.x
596   Chuine, I., Régnière, J., 2017. Process-Based Models of Phenology for Plants and Animals. Annu. Rev.
597   Ecol. Evol. Syst. 48, 159–182. https://doi.org/10.1146/annurev-ecolsys-110316-022706
598   Clark, J.S., Melillo, J., Mohan, J., Salk, C., 2014a. The seasonal timing of warming that controls onset of
599   the growing season. Global Change Biology 20, 1136–1145. https://doi.org/10.1111/gcb.12420
600   Clark, J.S., Salk, C., Melillo, J., Mohan, J., 2014b. Tree phenology responses to winter chilling, spring
601   warming, at north and south range limits. Functional Ecology 28, 1344–1355.
602   https://doi.org/10.1111/1365-2435.12309
603   Črepinšek, Z., Kajfež-Bogataj, L., Bergant, K., 2006. Modelling of weather variability effect on
604   fitophenology. Ecological Modelling, Special Issue on the Fourth European Conference on
605   Ecological Modelling 194, 256–265. https://doi.org/10.1016/j.ecolmodel.2005.10.020
606   Friedl, M.A., Gray, J.M., Melaas, E.K., Richardson, A.D., Hufkens, K., Keenan, T.F., Amey Bailey,
607   O'Keefe, J., 2014. A tale of two springs: using recent climate anomalies to characterize the
608   sensitivity of temperate forest phenology to climate change. Environ. Res. Lett. 9, 054006.
609   https://doi.org/10.1088/1748-9326/9/5/054006
610   Fu, Y.H., Geng, X., Hao, F., Vitasse, Y., Zohner, C.M., Zhang, X., Zhou, X., Yin, G., Peñuelas, J., Piao,
611   S., Janssens, I.A., 2019. Shortened temperature-relevant period of spring leaf-out in temperate-
612   zone trees. Global Change Biology 25, 4282–4290. https://doi.org/10.1111/gcb.14782
613   Fu, Y.H., Zhao, H., Piao, S., Peaucelle, M., Peng, S., Zhou, G., Ciais, P., Huang, M., Menzel, A.,
614   Peñuelas, J., Song, Y., Vitasse, Y., Zeng, Z., Janssens, I.A., 2015. Declining global warming
615   effects on the phenology of spring leaf unfolding. Nature 526, 104–107.
616   https://doi.org/10.1038/nature15402
617   Gray, J., Sulla-Menashe, D., Friedl, M.A., 2019. User Guide to Collection 6 MODIS Land Cover
618   Dynamics (MCD12Q2) Product. https://doi.org/10.5067/MODIS/MCD12Q2.006
619   Güsewell, S., Furrer, R., Gehrig, R., Pietragalla, B., 2017. Changes in temperature sensitivity of spring
620   phenology with recent climate warming in Switzerland are related to shifts of the preseason.
621   Global Change Biology 23, 5189–5202. https://doi.org/10.1111/gcb.13781

622 Hänninen, H., Kramer, K., Tanino, K., Zhang, R., Wu, J., Fu, Y.H., 2019. Experiments Are Necessary in
623   Process-Based Tree Phenology Modelling. Trends in Plant Science 24, 199–209.
624   https://doi.org/10.1016/j.tplants.2018.11.006
625 Heide, O.M., Prestrud, A.K., 2005. Low temperature, but not photoperiod, controls growth cessation and
626   dormancy induction and release in apple and pear. Tree Physiology 25, 109–114.
627   https://doi.org/10.1093/treephys/25.1.109
628 Huang, Y., Jiang, N., Shen, M., Guo, L., 2020. Effect of preseason diurnal temperature range on the start
629   of vegetation growing season in the Northern Hemisphere. Ecological Indicators 112, 106161.
630   https://doi.org/10.1016/j.ecolind.2020.106161
631 Hufkens, K., Basler, D., Milliman, T., Melaas, E.K., Richardson, A.D., 2018. An integrated phenology
632   modelling framework in r. Methods in Ecology and Evolution 9, 1276–1285.
633   https://doi.org/10.1111/2041-210X.12970
634 Hunter, A.F., Lechowicz, M.J., 1992. Predicting the Timing of Budburst in Temperate Trees. Journal of
635   Applied Ecology 29, 597–604. https://doi.org/10.2307/2404467
636 Jackson, S.D., 2009. Plant responses to photoperiod. New Phytologist 181, 517–531.
637   https://doi.org/10.1111/j.1469-8137.2008.02681.x
638 Keenan, T.F., Gray, J., Friedl, M.A., Toomey, M., Bohrer, G., Hollinger, D.Y., Munger, J.W., O'Keefe, J.,
639   Schmid, H.P., Wing, I.S., Yang, B., Richardson, A.D., 2014. Net carbon uptake has increased
640   through warming-induced changes in temperate forest phenology. Nature Climate Change 4,
641   598–604. https://doi.org/10.1038/nclimate2253
642 Keenan, T.F., Richardson, A.D., Hufkens, K., 2019. On quantifying the apparent temperature sensitivity
643   of plant phenology. New Phytol nph.16114. https://doi.org/10.1111/nph.16114
644 Körner, C., Basler, D., 2010. Phenology Under Global Warming. Science 327, 1461–1462.
645   https://doi.org/10.1126/science.1186473
646 Laube, J., Sparks, T.H., Estrella, N., Höfler, J., Ankerst, D.P., Menzel, A., 2014. Chilling outweighs
647   photoperiod in preventing precocious spring development. Global Change Biology 20, 170–182.
648   https://doi.org/10.1111/gcb.12360
649 Liu, Q., Fu, Y.H., Liu, Y., Janssens, I.A., Piao, S., 2017. Simulating the onset of spring vegetation growth
650   across the Northern Hemisphere. Global Change Biology 24, 1342–1356.
651   https://doi.org/10.1111/gcb.13954
652 Masle, J., Doussinault, G., Farquhar, G.D., Sun, B., 1989. Foliar stage in wheat correlates better to
653   photothermal time than to thermal time. Plant, Cell & Environment 12, 235–247.
654   https://doi.org/10.1111/j.1365-3040.1989.tb01938.x
655 Melaas, E.K., Richardson, A.D., Friedl, M.A., Dragoni, D., Gough, C.M., Herbst, M., Montagnani, L.,
656   Moors, E., 2013. Using FLUXNET data to improve models of springtime vegetation activity
657   onset in forest ecosystems. Agricultural and Forest Meteorology 171–172, 46–56.
658   https://doi.org/10.1016/j.agrformet.2012.11.018
659 Melaas, E.K., Sulla-Menashe, D., Friedl, M.A., 2018. Multidecadal Changes and Interannual Variation in
660   Springtime Phenology of North American Temperate and Boreal Deciduous Forests. Geophysical
661   Research Letters 45, 2679–2687. https://doi.org/10.1002/2017GL076933
662 Menzel, A., Sparks, T.H., Estrella, N., Koch, E., Aasa, A., Ahas, R., Alm-Kübler, K., Bissolli, P.,
663   Braslavská, O., Briede, A., Chmielewski, F.M., Crepinsek, Z., Curnel, Y., Dahl, Å., Defila, C.,
664   Donnelly, A., Filella, Y., Jatczak, K., Måge, F., Mestre, A., Nordli, Ø., Peñuelas, J., Pirinen, P.,
665   Remišová, V., Scheifinger, H., Striz, M., Susnik, A., Vliet, A.J.H.V., Wielgolaski, F.-E., Zach, S.,
666   Zust, A., 2006. European phenological response to climate change matches the warming pattern.
667   Global Change Biology 12, 1969–1976. https://doi.org/10.1111/j.1365-2486.2006.01193.x
668 Migliavacca, M., Sonnentag, O., Keenan, T.F., Cescatti, A., O&apos;Keefe, J., Richardson, A.D.,
669   2012. On the uncertainty of phenological responses to climate change, and implications for a
670   terrestrial biosphere model. Biogeosciences 9, 2063–2083. https://doi.org/10.5194/bg-9-2063-
671   2012

672   Montgomery, R.A., Rice, K.E., Stefanski, A., Rich, R.L., Reich, P.B., 2020. Phenological responses of
673   temperate and boreal trees to warming depend on ambient spring temperatures, leaf habit, and
674   geographic range. Proc Natl Acad Sci USA 201917508. https://doi.org/10.1073/pnas.1917508117
675   Moon, M., Li, D., Liao, W., Rigden, A.J., Friedl, M.A., 2020. Modification of surface energy balance
676   during springtime: The relative importance of biophysical and meteorological changes.
677   Agricultural and Forest Meteorology 284, 107905.
678   https://doi.org/10.1016/j.agrformet.2020.107905
679   Moon, M., Zhang, X., Henebry, G.M., Liu, L., Gray, J.M., Melaas, E.K., Friedl, M.A., 2019. Long-term
680   continuity in land surface phenology measurements: A comparative assessment of the MODIS
681   land cover dynamics and VIIRS land surface phenology products. Remote Sensing of
682   Environment 226, 74–92. https://doi.org/10.1016/j.rse.2019.03.034
683   Murray, M.B., Cannell, M.G.R., Smith, R.I., 1989. Date of Budburst of Fifteen Tree Species in Britain
684   Following Climatic Warming. Journal of Applied Ecology 26, 693–700.
685   https://doi.org/10.2307/2404093
686   Park, T., Chen, C., Macias-Fauria, M., Tømmervik, H., Choi, S., Winkler, A., Bhatt, U.S., Walker, D.A.,
687   Piao, S., Brovkin, V., Nemani, R.R., Myneni, R.B., 2019. Changes in timing of seasonal peak
688   photosynthetic activity in northern ecosystems. Glob Change Biol gcb.14638.
689   https://doi.org/10.1111/gcb.14638
690   Parmesan, C., Yohe, G., 2003. A globally coherent fingerprint of climate change impacts across natural
691   systems. Nature 421, 37–42. https://doi.org/10.1038/nature01286
692   Peñuelas, J., Rutishauser, T., Filella, I., 2009. Phenology Feedbacks on Climate Change. Science 324,
693   887–888. https://doi.org/10.1126/science.1173004
694   Piao, S., Liu, Q., Chen, A., Janssens, I.A., Fu, Y., Dai, J., Liu, L., Lian, X., Shen, M., Zhu, X., 2019. Plant
695   phenology and global climate change: current progresses and challenges. Global Change Biology.
696   https://doi.org/10.1111/gcb.14619
697   Piao, S., Liu, Z., Wang, T., Peng, S., Ciais, P., Huang, M., Ahlstrom, A., Burkhart, J.F., Chevallier, F.,
698   Janssens, I.A., Jeong, S.-J., Lin, X., Mao, J., Miller, J., Mohammat, A., Myneni, R.B., Peñuelas,
699   J., Shi, X., Stohl, A., Yao, Y., Zhu, Z., Tans, P.P., 2017. Weakening temperature control on the
700   interannual variations of spring carbon uptake across northern lands. Nature Climate Change 7,
701   359–363. https://doi.org/10.1038/nclimate3277
702   Piao, S., Tan, J., Chen, A., Fu, Y.H., Ciais, P., Liu, Q., Janssens, I.A., Vicca, S., Zeng, Z., Jeong, S.-J., Li,
703   Y., Myneni, R.B., Peng, S., Shen, M., Peñuelas, J., 2015. Leaf onset in the northern hemisphere
704   triggered by daytime temperature. Nature Communications 6, 6911.
705   https://doi.org/10.1038/ncomms7911
706   Qiu, T., Song, C., Clark, J.S., Seyednasrollah, B., Rathnayaka, N., Li, J., 2020. Understanding the
707   continuous phenological development at daily time step with a Bayesian hierarchical space-time
708   model: impacts of climate change and extreme weather events. Remote Sensing of Environment
709   247, 111956. https://doi.org/10.1016/j.rse.2020.111956
710   Richardson, A.D., Hufkens, K., Milliman, T., Aubrecht, D.M., Furze, M.E., Seyednasrollah, B.,
711   Krassovski, M.B., Latimer, J.M., Nettles, W.R., Heiderman, R.R., Warren, J.M., Hanson, P.J.,
712   2018a. Ecosystem warming extends vegetation activity but heightens vulnerability to cold
713   temperatures. Nature. https://doi.org/10.1038/s41586-018-0399-1
714   Richardson, A.D., Hufkens, K., Milliman, T., Frolking, S., 2018b. Intercomparison of phenological
715   transition dates derived from the PhenoCam Dataset V1.0 and MODIS satellite remote sensing.
716   Scientific Reports 8, 5679. https://doi.org/10.1038/s41598-018-23804-6
717   Richardson, A.D., Keenan, T.F., Migliavacca, M., Ryu, Y., Sonnentag, O., Toomey, M., 2013. Climate
718   change, phenology, and phenological control of vegetation feedbacks to the climate system.
719   Agricultural and Forest Meteorology 169, 156–173.
720   https://doi.org/10.1016/j.agrformet.2012.09.012

721 Rosemartin, A.H., Denny, E.G., Weltzin, J.F., Lee Marsh, R., Wilson, B.E., Mehdipoor, H., Zurita-Milla,
722   R., Schwartz, M.D., 2015. Lilac and honeysuckle phenology data 1956–2014. Scientific Data 2,
723   150038. https://doi.org/10.1038/sdata.2015.38
724 Schewe, J., Gosling, S.N., Reyer, C., Zhao, F., Ciais, P., Elliott, J., Francois, L., Huber, V., Lotze, H.K.,
725   Seneviratne, S.I., van Vliet, M.T.H., Vautard, R., Wada, Y., Breuer, L., Büchner, M., Carozza,
726   D.A., Chang, J., Coll, M., Deryng, D., de Wit, A., Eddy, T.D., Folberth, C., Frieler, K., Friend,
727   A.D., Gerten, D., Gudmundsson, L., Hanasaki, N., Ito, A., Khabarov, N., Kim, H., Lawrence, P.,
728   Morfopoulos, C., Müller, C., Müller Schmied, H., Orth, R., Ostberg, S., Pokhrel, Y., Pugh,
729   T.A.M., Sakurai, G., Satoh, Y., Schmid, E., Stacke, T., Steenbeek, J., Steinkamp, J., Tang, Q.,
730   Tian, H., Tittensor, D.P., Volkholz, J., Wang, X., Warszawski, L., 2019. State-of-the-art global
731   models underestimate impacts from climate extremes. Nature Communications 10, 1005.
732   https://doi.org/10.1038/s41467-019-08745-6
733 Schwartz, M.D., Ahas, R., Aasa, A., 2006. Onset of spring starting earlier across the Northern
734   Hemisphere. Global Change Biology 12, 343–351. https://doi.org/10.1111/j.1365-
735   2486.2005.01097.x
736 Senf, C., Pflugmacher, D., Heurich, M., Krueger, T., 2017. A Bayesian hierarchical model for estimating
737   spatial and temporal variation in vegetation phenology from Landsat time series. Remote Sensing
738   of Environment 194, 155–160. https://doi.org/10.1016/j.rse.2017.03.020
739 Seyednasrollah, B., Swenson, J.J., Domec, J.-C., Clark, J.S., 2018. Leaf phenology paradox: Why
740   warming matters most where it is already warm. Remote Sensing of Environment 209, 446–455.
741   https://doi.org/10.1016/j.rse.2018.02.059
742 Seyednasrollah, B., Young, A.M., Li, X., Milliman, T., Ault, T., Frolking, S., Friedl, M., Richardson,
743   A.D., 2020. Sensitivity of Deciduous Forest Phenology to Environmental Drivers: Implications
744   for Climate Change Impacts Across North America. Geophys. Res. Lett. 47.
745   https://doi.org/10.1029/2019GL086788
746 Shen, X., Liu, B., Henderson, M., Wang, L., Wu, Z., Wu, H., Jiang, M., Lu, X., 2018. Asymmetric effects
747   of daytime and nighttime warming on spring phenology in the temperate grasslands of China.
748   Agricultural and Forest Meteorology 259, 240–249.
749   https://doi.org/10.1016/j.agrformet.2018.05.006
750 Su, Y.-S., Yajima, M., 2015. R2jags: Using R to Run "JAGS".
751 Sulla-Menashe, D., Gray, J.M., Abercrombie, S.P., Friedl, M.A., 2019. Hierarchical mapping of annual
752   global land cover 2001 to present: The MODIS Collection 6 Land Cover product. Remote
753   Sensing of Environment 222, 183–194. https://doi.org/10.1016/j.rse.2018.12.013
754 Thornton, P.E., Thornton, M.M., Mayer, B.W., Wei, Y., Devarakonda, R., Vose, R.S., Cook, R.B., 2017.
755   Daymet: Daily Surface Weather Data on a 1-km Grid for North America, Version 3.
756   https://doi.org/10.3334/ORNLDAAC/1328
757 Walther, G.-R., Post, E., Convey, P., Menzel, A., Parmesan, C., Beebee, T.J.C., Fromentin, J.-M., Hoegh-
758   Guldberg, O., Bairlein, F., 2002. Ecological responses to recent climate change. Nature 416, 389–
759   395. https://doi.org/10.1038/416389a
760 Wenden, B., Mariadassou, M., Chmielewski, F.-M., Vitasse, Y., 2020. Shifts in the temperature-sensitive
761   periods for spring phenology in European beech and pedunculate oak clones across latitudes and
762   over recent decades. Global Change Biology 26, 1808–1819. https://doi.org/10.1111/gcb.14918
763 Wolkovich, E.M., Cook, B.I., Allen, J.M., Crimmins, T.M., Betancourt, J.L., Travers, S.E., Pau, S.,
764   Regetz, J., Davies, T.J., Kraft, N.J.B., Ault, T.R., Bolmgren, K., Mazer, S.J., McCabe, G.J.,
765   McGill, B.J., Parmesan, C., Salamin, N., Schwartz, M.D., Cleland, E.E., 2012. Warming
766   experiments underpredict plant phenological responses to climate change. Nature 485, 494–497.
767   https://doi.org/10.1038/nature11014
768 Zhang, X., Liu, L., Liu, Y., Jayavelu, S., Wang, J., Moon, M., Henebry, G.M., Friedl, M.A., Schaaf, C.B.,
769   2018. Generation and evaluation of the VIIRS land surface phenology product. Remote Sensing
770   of Environment 216, 212–229. https://doi.org/10.1016/j.rse.2018.06.047

771   Zohner, C.M., Benito, B.M., Svenning, J.-C., Renner, S.S., 2016. Day length unlikely to constrain
772   climate-driven shifts in leaf-out times of northern woody plants. Nature Climate Change 6, 1120–
773   1123. https://doi.org/10.1038/nclimate3138
774

775

798 time model; PTT: The photo-thermal time model; TT: The thermal time model; AT: The

799 alternating model. Boxplots are presented in increasing order of magnitude with respect to mean

800 RMSE.

801

802 **Fig. 4.** Geographic variation in the dependence of spring greenup onset date to: (a) thermal

803 forcing, (b) photoperiod, and (c) chilling units. In panel (d), boxplots show the distribution of

804 model coefficients for each control variable during the pre-season period prior to leaf emergence

805 in Northern Forests (blue) versus Eastern Temperate Forests (red). Differences between the

806 means in both cases are statistically significant ($p < 0.001$).

807

808 **Fig. 5.** Relative importance (*RI*) of thermal forcing versus photoperiod. Circles in red and blue

809 show locations where thermal forcing and photoperiod, respectively, exert stronger control on

810 the timing of spring greenup; purple circles identify locations where the magnitude of thermal

811 forcing and photoperiod are roughly equivalent. The size of each circle is proportional to the

812 magnitude of *RI* in each cell.

813

814 **Fig. 6.** Dependence of cloned lilac leaf unfolding date on thermal forcing and photoperiod, and

815 relative importance (*RI*). 254 total leaf unfolding dates from cloned lilac were divided into two

816 groups based on mean annual temperature (≤ 10 ºC, $n = 182$; > 10 ºC, $n = 72$). The left panel

817 plots the mean dependence of leaf unfolding on thermal forcing and photoperiod estimated by

818 the CDSOM. The right panel plots the mean *RI* in each group. Positive *RI* indicates stronger

819 control by thermal forcing relative to photoperiod. Vertical lines show ±1 standard deviation.

821 **Fig. 7.** Variation in pre-season period and the relationship between greenup dependence on

822 photoperiod and length of pre-season period. (a) Geographic pattern in pre-season period, and (b)

823 log-log relationship between the dependence of greenup on photoperiod and the length of the

824 pre-season period.

825

826 **Fig. A1.** Map of the study area. Extents of the US EPA Northern Forest and Eastern Temperate

827 Forest ecoregions, along with the proportion 500 m MODIS pixels labeled as deciduous forests

828 in each grid cell according to the Collection 6 MODIS Land Cover Type product. Red crosses

829 show the USA-National Phenology Network site locations where lilac data are collected. Note

830 that because the MODIS Land Cover Type product uses a threshold of 60% cover to define

831 forest classes, the map shown in Fig. A1 modestly over-represents the actual proportion of

832 deciduous forest cover.

833

834 **Fig. A2.** Relationship between anomalies in MODIS onset dates and anomalies in model-

835 predicted onset dates. Panels (a)-(e) show results for the Continuous Development Spring Onset

836 Model (CDSOM), the thermal time model (TT), the photo-thermal time model (PTT), the

837 exponential photo-thermal time model (M1), and the alternating model (AT), respectively.

838 Dashed lines and correlation coefficients (r) show the results from standard major axis regression.

839

840 **Fig. A3.** Relationship between MODIS greenup dates and leaf unfolding dates from the USA-

841 NPN cloned lilac dataset. The colder (red dots) and warmer (blue dots) sites are divided based on

842 mean annual temperature (i.e., colder $\leq$ 10 ℃; warmer > 10 ℃). n (= 198) is different from the

843 total number of USA-NPN leaf unfolding dates (n = 254) due to cases where no MODIS dates

844 were available because the lilac site was not located in a location dominated by deciduous or

845 mixed forest at the scale of MODIS pixels.

846

847 **Fig. A4.** Relationship between pre-season period length and dependence on thermal forcing.

848